

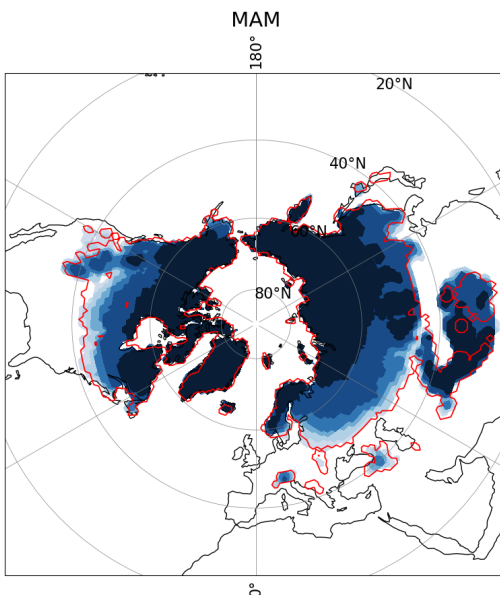
University Grenoble Alpes
PhITEM

M2 - SCAHC

2024-2025

Long Internship

Study of the spatial distribution of snow as a function of global warming



Author:

Laurie VAYSSETTES - 12304985

Tutor:

Dr. Gerhard KRINNER

Date:

17th February - 31st July 2025

Certificate of non-plagiarism

I, the undersigned VAYSSETTES Laurie declares on his honor that this report is the result of a personal work and that I have neither counterfeited, falsified or copied all or part of the work of another in order to pass it off as mine.

All sources of information used (paper, audiovisual, and digital) and author citations have been mentioned in accordance with current practice.

I am aware that the failure to cite a source or to cite it clearly and completely constitutes plagiarism, that plagiarism is considered a serious misconduct within the University Grenoble Alpes and that it can be severely sanctioned.

Date: 10/06/2025**Signature of the Candidate**A handwritten signature in black ink, appearing to read "Vayssettes", is written over a diagonal line. The signature is somewhat stylized and includes a small cross-like mark at the end.

Acknowledgments

I would like to sincerely thank the hosting laboratory, the IGE, for providing a great environment to carry out this internship. Special thanks go to my supervisor, Gerhard Krinner, for his guidance and support throughout the project.

I am also grateful to Martin Menegoz for lending me a computer, which was very useful, and to Charles Amory for kindly providing me with a workspace. I would like to thank the IT services for their quick responses and efforts in getting a working computer set up as soon as possible.

This research internship benefited from the support of the laboratory's digital platform, as part of the OpenReproLab initiative. The students had access to a cloud-based computing environment. They also took part in weekly training sessions focused on coding practices and data management aimed at improving the reproducibility of results. These trainings, along with support throughout the internship from members of the digital platform, introduced tools, methods, and a work organization that promote direct integration of the project into the methodologies and best practices to deliver open and reproducible science. In particular, I want to mention Aurélie, and Mykaël—thank you for helping me solve some coding problems—and many others whose collaboration and discussions were very valuable.

I would like to thank Maria Santolaria-Otin for sharing her data, and Nicolas Jourdain for agreeing to be my report reviewer.

Finally, I am grateful to UGA for the opportunity to complete this internship and for the efficiency of the administrative process.

Abstract

Snow and sea ice respond rapidly to atmospheric warming, making them critical indicators of climate change. This study presents new maps of snow cover extent at different Global Warming Levels (GWLs), derived from a multi-model average of CMIP6 simulations. The GWL approach offers a more direct link between temperature rise and snow cover changes than traditional scenario-based methods. We explore how key methodological choices—such as the snow variable selected (snow cover fraction vs. snow mass), model selection and weighting, and the snow presence threshold—impact projection results. Using snow cover fraction, which closely relates to the surface energy balance, helps maintain consistency with climate feedback processes. However, the degree of model agreement varies depending on how snow is defined and the threshold applied. A 15% threshold, commonly used in sea ice studies, proves suitable for snow cover as well. Our results reveal a marked and non-linear decline in snow cover between +3°C and +4°C warming relative to 1995–2014. This highlights the importance of adopting a GWL-based framework for evaluating future snow cover changes.

Key words: CMIP6, snow, snow cover fraction, global warming levels (GWLs), climate projections, climate variability, cryosphere

La neige et la banquise réagissent rapidement au réchauffement atmosphérique, ce qui en fait des indicateurs clés du changement climatique. Cette étude propose de nouvelles cartes de l'étendue de la couverture neigeuse selon différents niveaux de réchauffement global (Global Warming Levels, GWLs), obtenues à partir de la moyenne multi-modèles des simulations CMIP6. L'approche basée sur les GWL permet d'établir un lien plus direct entre la hausse des températures et les variations de la neige que les méthodes traditionnelles fondées sur des scénarios. Nous étudions comment certaines décisions méthodologiques — le choix de la variable neige (fraction de couverture neigeuse vs. masse de neige), la sélection et la pondération des modèles, ainsi que le seuil de présence de la neige — influent sur les projections. L'utilisation de la fraction de couverture neigeuse, liée directement au bilan d'énergie à la surface, garantit une cohérence avec les processus de rétroaction climatique. Toutefois, l'accord entre modèles dépend de la définition de la neige et du seuil retenu. Un seuil de 15%, couramment utilisé pour la banquise, apparaît pertinent pour la neige également. Nos résultats montrent une forte diminution, non linéaire, de la couverture neigeuse entre +3°C et +4°C de réchauffement par rapport à la période 1995–2014. Ces observations soulignent l'intérêt d'une approche basée sur les GWL pour mieux évaluer les changements futurs de la neige.

Mots clés: CMIP6, neige, fraction de couverture neigeuse, niveaux de réchauffement global (GWLs), projections climatiques, variabilité climatique, cryosphère

Contents

Acknowledgments	2
Abstract	3
1 Introduction	5
2 Data and Methods	7
2.1 Data	7
2.1.1 Model data	7
2.1.2 Reference data	8
2.2 Methods	10
2.2.1 Model selection	10
2.2.2 Multi-model means	12
2.2.3 OpenReproLab	13
3 Results	14
3.1 Model selection	14
3.1.1 Snow cover agreement	14
3.1.2 Outlier detection	16
3.1.3 Scoring results	18
3.2 Multi-model mean	19
3.2.1 Multi-model methods comparison	19
3.2.2 Seasonal snow extension	21
3.2.3 Seasonal snow cover with a selection of models	24
3.2.4 Evolution of the snow extent compared to 1850-1900 period	25
4 Discussion	27
4.1 Snow variables and representation issues in climate models	27
4.2 Final model selection and weighting strategy	27
4.3 Impact of snow threshold and model sampling on results	28
4.4 Scenario dependence and robustness of results	28
5 Conclusion and Outlooks	29
Bibliography	30
Annex	31

1 Introduction

Snow and sea ice are classified as “fast” climate variables, meaning they respond rapidly to atmospheric temperature fluctuations, on seasonal to decadal timescales, unlike other components such as continental ice sheets (IPCC (2021)). These cryospheric surfaces are particularly sensitive to temperature change, especially in transitional seasons and mid-elevation areas, where even modest warming can lead to a significant reduction in snow cover duration (Mudryk et al. (2020)). Arctic sea ice, similarly, has declined rapidly since the late 1970s, with an accelerated trend in summer, in direct response to Arctic amplification (IPCC (2021)). In CMIP6 (Eyring et al. (2016)) projections, spring snow cover extent declines almost linearly with increasing global surface air temperature and independently of the specific emissions scenario, reflecting its high sensitivity to warming (fig. 1).

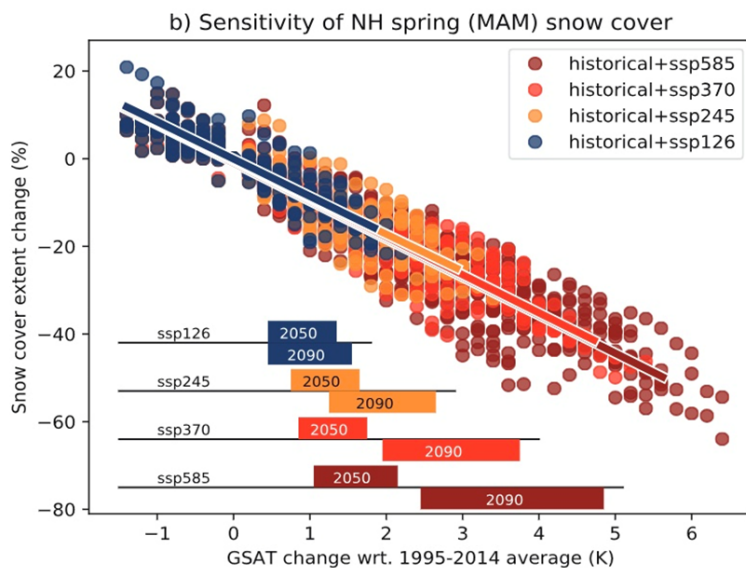


Figure 1: Spring (March to May) Northern Hemisphere snow cover extent change for the CMIP6 scenarios (Fig. 9.24, IPCC (2021))

In addition to being indicators of climate change, snow and sea ice play an essential role in climate feedbacks, notably via the surface albedo effect, amplifying warming in high latitudes. Their future evolution is therefore a key concern for both regional and global climate projections.

Earth system models typically simulate climate trajectories from the pre-industrial period (1850–1900) through to 2100 and beyond, as illustrated for example in fig. 2. These simulations follow predefined emissions pathways known as Shared Socioeconomic Pathways (SSPs), which pair societal development scenarios with corresponding greenhouse gas trajectories. For instance, SSP1-2.6 represents a sustainable world with low emissions, while SSP5-8.5 reflects a fossil-fuel intensive future. However, not all shared socioeconomic pathways are compatible with all emissions pathways. For example, SSP1 is incompatible with high emissions, while SSP3 cannot realistically achieve low emissions.

More recently, there has been a shift in the way these simulations are analyzed : rather than focusing only on future time periods or specific scenarios, scientists increasingly evaluate model outputs based on Global Warming Levels (GWLs, see IPCC (2021), Box 11.1). This approach aligns analyses with specific levels of global mean temperature rise relative to the pre-industrial era (e.g., +1.5°C, +3°C...), regardless of the specific SSP or year in which that warming level is reached

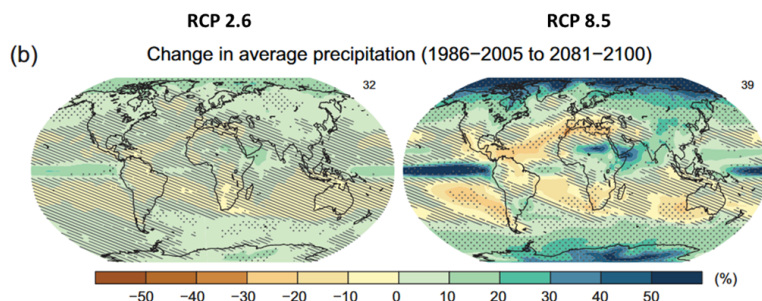


Figure 2: Average percent change in annual mean precipitation projected from the CMIP5 ensemble for different scenarios (Figure SPM.8, IPCC SPM, WGI IPCC (2013))

(fig. 3). This method is more policy-relevant, as it directly addresses international climate goals, especially those set by the Paris Agreement, which aims to keep global warming “well below 2°C” and to “pursue efforts to limit it to 1.5°C”.

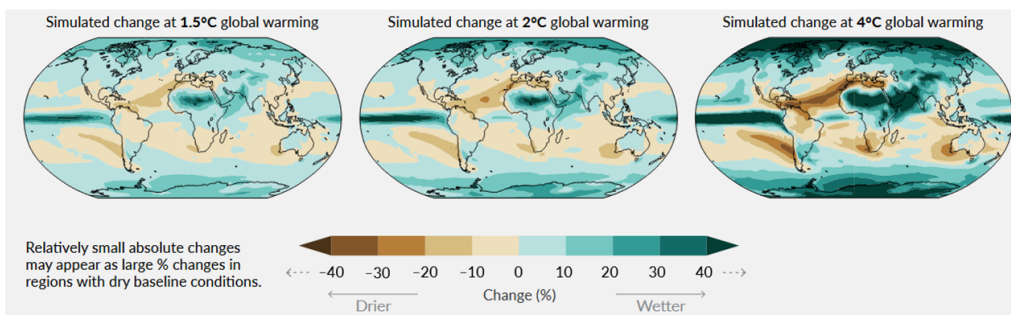


Figure 3: Projected changes in annual mean precipitation for different GWLs (Figure SPM.5, IPCC SPM, WGI AR6, 2021)

Analyzing climate impacts at these warming levels improves comparability across models and scenarios, and better reflects the climate system’s response to temperature rise, independently of socio-economic assumptions. This is particularly important for fast-reacting variables like snow and sea ice, whose distribution patterns are strongly related to “instantaneous” (e.g. monthly or seasonal) temperature.

The objective of this internship was to explore how the spatial distribution of snow cover and sea ice evolves in CMIP6 simulations as a function of global warming. To our knowledge, no study to date has published comprehensive maps showing snow extent as a function of global mean temperature on a single figure. The main goal of this internship was therefore to produce such maps. By comparing both historical and future outputs from climate models, the work aimed to evaluate how accurately models reproduce observed patterns and to analyze projected changes across different levels of global temperature increase. The final results, presented in the form of maps, are based on a selection of climate models and the computation of a multi-model mean from this subset. A central question addressed throughout the internship is whether producing a multi-model mean is scientifically justified and whether such an approach yields reliable insights. Although sea ice is frequently used in the introduction to illustrate key concepts, the analysis and results presented in this report focus exclusively on snow cover simulations.

Finally, this work adheres to the principles of open science and scientific reproducibility. In an

era where methodological transparency, open access to data and code, and the ability to reproduce results have become fundamental in scientific research, this internship aimed to document each step of the analysis and to ensure that all scripts and figures are reproducible. This approach is useful to keep a scientific quality of the results and make the work reproducible for the whole community.

This report is structured as follows. The first part presents the data and methods used, including the criteria for model selection and the various processing steps. The second part focuses on the results, beginning with model evaluation based on snow cover agreement and the identification of outliers. This is followed by a presentation of the multi-model mean results, first over the reference period using different methods, and then for future snow cover extent projections relative to both 1995-2014 and 1850-1900. The third part provides discussion of the methodological choices and the main findings. Finally, the report concludes with some outlooks and potential future directions for this work.

2 Data and Methods

2.1 Data

2.1.1 Model data

A large volume of data (approximately 40 Go) was used to perform the various analyses. Most of the datasets were accessed through the ESPRI Mesocenter of the Institut Pierre-Simon Laplace, which requires authorization for use (<https://mesocentre.ipsl.fr/>). All the data are provided by the Coupled Model Intercomparison Project Phase 6 (CMIP6).

For our analysis, we used several types of data. Historical and projection datasets were both utilized, retrieved from the CMIP (historical runs) and ScenarioMIP directories, respectively. Within these folders, we focused on specific variables: surface air temperature (tas) and snow cover (snc) for both the historical and future periods. For future projections, we concentrated on the SSP5-8.5 scenario, as it represents the most extreme and long-term evolution among the scenarios, and because of scenario independency of seasonal snow cover (Mudryk et al. (2020)).

These variables were collected across all CMIP6 models. Table 1 lists the models and their corresponding institutions. In total, 25 models include snow cover. For each model and variable, multiple realizations were available (e.g., r1i1p1f1). This notation follows the CMIP6 convention, where each letter refers to a specific aspect of the simulation configuration : r indicates the ensemble member which correspond to different initial conditions; i is the initialization method; p refers to the physical parameter set used in the model (for example, variations in cloud parameterizations), with p1 generally considered the standard version; and f represents the forcing configuration, which can differ in terms of external forcing datasets, such as aerosols or solar irradiance, particularly relevant for long simulations where uncertainties increase. We consistently selected the realization closest to the first one available.

Additionally, we used complementary data for each model: areacella (providing the surface area

of each grid cell), sftlf (land area fraction), and sftgif (land ice area fraction). All datasets were in NetCDF format.

For historical simulations, we also used the snow mass variable (snw) in order to recalculate the snow cover based on a threshold value. This variable was available for most models, although it was missing for two of them (FGOALS-f3-L and FGOALS-g3), which were therefore excluded from the related analyses.

2.1.2 Reference data

The snow reference data used in this study come from the Rutgers University dataset (<https://climate.rutgers.edu/snowcover/>), regridded onto a $1^\circ \times 1^\circ$ grid (Estilow et al. (2015)). This interpolation was performed using a reference grid specifically created for this purpose. The dataset covers the period from 1980 to the present, but for our analysis, we use the reference period defined by the IPCC, which spans from 1995 to 2014. It is important to note that the snow extent data provided by this dataset are limited to the Northern Hemisphere. This focus is common in the literature, as snow in the Southern Hemisphere is rarely analyzed in detail in most studies, including the IPCC reports. Although the Rutgers dataset is widely used in climatology and provides reliable information on snow cover extent, it has known limitations when it comes to long-term trends in autumn, as highlighted by Mudryk et al. (2020). However, since this study does not focus on trend analysis, the dataset remains appropriate for our purposes.

Model name(s)	Modeling center
BCC-CSM2-MR	Beijing Climate Center Climate System Model (China)
CESM2, CESM2-WACCM	Community Earth System Model 2 / CESM2-Whole Atmosphere Community Climate Model
CIESM	Community Integrated Earth System Model (China)
CNRM-CM6-1, CNRM-CM6-1-HR, CNRM-ESM2-1	Centre National de Recherches Météorologiques / Centre Européen de Recherche et Formation Avancée en Calcul Scientifique (CNRM-CERFACS) (France)
CanESM5, CanESM5-CanOE	Canadian Earth System Model version 5 / Canadian Ocean Ecosystem Model
EC-Earth3, EC-Earth3-Veg	EC-Earth Consortium
FGOALS-f3-L, FGOALS-g3	Laboratory of Numerical Modeling for Atmospheric Sciences and Geophysical Fluid Dynamics (LASG) (China)
GFDL-CM4	National Oceanic and Atmospheric Administration (NOAA, USA)
GISS-E2-1-G	Goddard Institute for Space Studies (NASA-GISS, USA)
HadGEM3-GC31-LL, UKESM-1-0-LL	Met Office Hadley Centre (MOHC, UK)
IPSL-CM6A-LR	Institut Pierre Simon Laplace (France)
MIROC-ES2L, MIROC6	JAMSTEC / AORI / NIES / RIKEN Center for Computational Science (Japan)
MPI-ESM1-2-HR, MPI-ESM1-2-LR	Max Planck Institute for Meteorology (Germany)
MRI-ESM2-0	Meteorological Research Institute (Japan)
NorESM2-LM, NorESM2-MM	Norwegian Climate Centre

Table 1: Model name and modelling center for whole the models used (World Data Center for Climate)

2.2 Methods

Before proceeding with the analysis, several preprocessing steps were necessary. The first step was to regrid all datasets onto a common reference grid to enable consistent comparisons across models. This grid uses a regular latitude-longitude format with a $1^\circ \times 1^\circ$ resolution, covering the globe from -179.5° to $+179.5^\circ$ in longitude and -89.5° to $+89.5^\circ$ in latitude. This is the same grid used in the Rutgers dataset, ensuring compatibility. Regridding was performed using a nearest-neighbour source-to-destination interpolation method (nearest s2d). A verification step was performed to ensure that the regridding process was reliable. For instance, one comparison showed that the difference in continental area between the original and regridded files was around 1%, which is considered negligible.

As the focus of our study is on seasonal snow, the analysis was restricted to the Northern Hemisphere, and we chose to limit the study area to latitudes north of approximately 20°N . Greenland was retained, as it is included in the Rutgers dataset. For the IPSL model specifically, we had to restore Greenland using the model's land-ice mask, since snow cover was not defined on ice sheets in the CMIP6 repository for this model.

2.2.1 Model selection

To select suitable models from the available CMIP6 ensemble, we compared the monthly snow extent simulated by each model with the reference dataset. This comparison allowed us to assess which models closely follow observed values and which deviate significantly.

Two different methods were used for this evaluation.

- The first approach involved analyzing the historical simulations, focusing on the “present” reference period used by the IPCC for model evaluation (1995–2014).
- The second method used the output from the first step but examined the data based on the level of global warming. According to the IPCC (IPCC (2021)), the global mean temperature increase for the period 1995–2014, relative to 1850–1900, was approximately $+0.85^\circ\text{C}$. In this second approach, we selected, for each model, the 20-year period during which the global mean temperature reached $+0.85^\circ\text{C}$ above that model's 1850–1900 average. This period does not necessarily correspond to 1995–2014; it may occur earlier or later depending on the model. Monthly snow extent was then calculated over this warming-aligned period.

One common source of error among models is the misestimation of the global warming level. In this context, the $+0.85^\circ\text{C}$ warming threshold used in our study may correspond to different time periods across models occurring earlier or later than the reference period. This temporal mismatch introduces uncertainty, making the warming-level-based approach more risky.

Finally, graphical visualizations were produced to help identify potential outliers through visual inspection. The first approach provides a spatial overview by counting, at each grid cell, the number of models that simulate snow. This method offers a quick and intuitive way to evaluate the overall

agreement among models and to spot areas where certain models might perform poorly, without relying on numerical metrics.

The second approach is more statistical, as it focuses on the distribution of numerical values to quickly highlight outliers. Among the different visualizations tested, such as violin plots, boxplots were selected for their clarity and effectiveness. These boxplots provide a concise summary of the snow cover extent distribution and allow for easy identification of anomalous model behavior.

Although the main analysis relies on the snow cover fraction variable, we also conducted a complementary comparison using the snow mass variable over the historical period. Following the approach proposed by Brutel-Vuilmet et al. (2013), we assumed snow to be present when the snow mass exceeds 5 kg.m² in a given month. This threshold allowed us to reconstruct a binary snow cover map from snw, which was then compared to the snc-based snow cover across models in order to assess consistency and evaluate model differences.

$$\text{Snow extent (km}^2\text{)} = \text{snc} \times (\text{areacella}/10^6) \quad (1)$$

Based on these results, both absolute and relative errors were calculated with respect to the reference dataset. These errors were then visualized using heat maps for each method, providing a clear and accessible way to interpret the model performances. A heatmap is a 2-dimensional data visualization tool that represents the magnitude of each value in the dataset using a color gradient. In our case, this was applied across all models and months. The color scale, ranging from white (low error) to red (high error) allows us to immediately identify which models and which months show the largest deviations. This visual approach makes it easy to quickly detect where errors are most pronounced.

$$\text{Absolute error (km}^2\text{)} = |\text{Snow extent}_{\text{model}} - \text{Snow extent}_{\text{obs}}| \quad (2)$$

$$\text{Relative error (\%)} = \frac{|\text{Snow extent}_{\text{model}} - \text{Snow extent}_{\text{obs}}|}{|\text{Snow extent}_{\text{obs}}|} \times 100 \quad (3)$$

Following the error analysis, a ranking of the models was carried out to support the selection process. This ranking was based on the previously absolute errors. The principle behind the ranking is simple: each model was assigned a score reflecting its ability to reproduce observed conditions. In general, the lower the error, the higher the score. Scores ranged from 0 (poor performance) to 1 (good performance).

Two different methods were tested to calculate the scores: one based on an exponential function, and the other on a Gaussian-style function.

$$\text{Score}_{\text{exp}} = \exp \left(-\frac{\text{Error}_{\text{model}} - \min(\text{Error})}{\max(\text{Error}) - \min(\text{Error})} \right) \quad (4)$$

$$\text{Score}_{\text{gauss-style}} = \exp \left(-\frac{(\text{Error}_{\text{model}} - m)^2}{2s^2} \right) \quad (5)$$

$$m = \min(\text{Error}) \quad s = \frac{\max(\text{Error}) - \min(\text{Error})}{4} \quad (6)$$

In the following, the Gaussian-style function will be referred to simply as the Gaussian function for clarity. Although it resembles the standard Gaussian distribution, it differs in that the parameters m and s were not computed in the same way as classic Gaussian functions. This choice was made to construct a scoring function that is well adapted to our ranking context. In particular, the parameter s was set to one quarter of the error range, ensuring a scoring curve that is both selective and smooth, while remaining easy to interpret.

After that, a visual verification was made to evaluate visually for the snow extent for certain models at 0, 20, 40, 60, 80 and 100% to make a decision for choosing the best scoring function. The selection of an appropriate scoring function depends on several criteria. First, it should assign high scores to the good models with scores that are consistent with the observed data, meaning that similar models (in terms of maps) receive similar scores, and dissimilar ones are scored accordingly. Conversely, poor models should receive low scores, ensuring they are not given importance. In this sense, a good scoring function is one that both rewards high-quality models and strongly discriminates against low-quality ones.

2.2.2 Multi-model means

Based on the previous results, we proceeded to construct multi-model means. Several approaches were tested.

The first method consisted of excluding the models that showed the poorest performance in reproducing snow extent. In contrast, the second approach involved weighting each model according to its score, in order to account for their varying levels of reliability. Two weighted means were computed: one using the Gaussian-based scoring, and the other using the exponential-based scoring.

$$\overline{\text{snc}} = \frac{1}{n} \sum_{i=1}^n \text{snc}_i \quad (7)$$

$$\overline{\text{snc}}_w = \frac{\sum_{i=1}^n w_i \text{snc}_i}{\sum_{i=1}^n w_i} \quad (8)$$

Finally, to create the snow cover maps, a binary mask was applied: grid cells with more than 15% snow cover were assigned a value of 1, and 0 otherwise. This choice comes from the fact that for the sea ice, this threshold is used a lot in some studies (Matthews et al. (2020)). Despite this final choice, some other tests were made before (notably at 50% snow cover). To avoid displaying snow over the ocean, a land-sea mask based on land fraction was used – only grid cells where the land fraction (sftlf) exceeds 50% were retained.

The final multi-model map of snow extent as a function of GWL is based on a binning procedure that involves several steps. First, the snow extent is identified separately for each global warming level. GWLs are defined with a resolution of 0.25°C , leading to a total of 23 levels. For each level, an individual snow cover map is generated. These maps are then summed to produce the final result. This process is illustrated in fig. 4 for one model. The same procedure was applied to all models, and a weighted multi-model mean was then calculated.

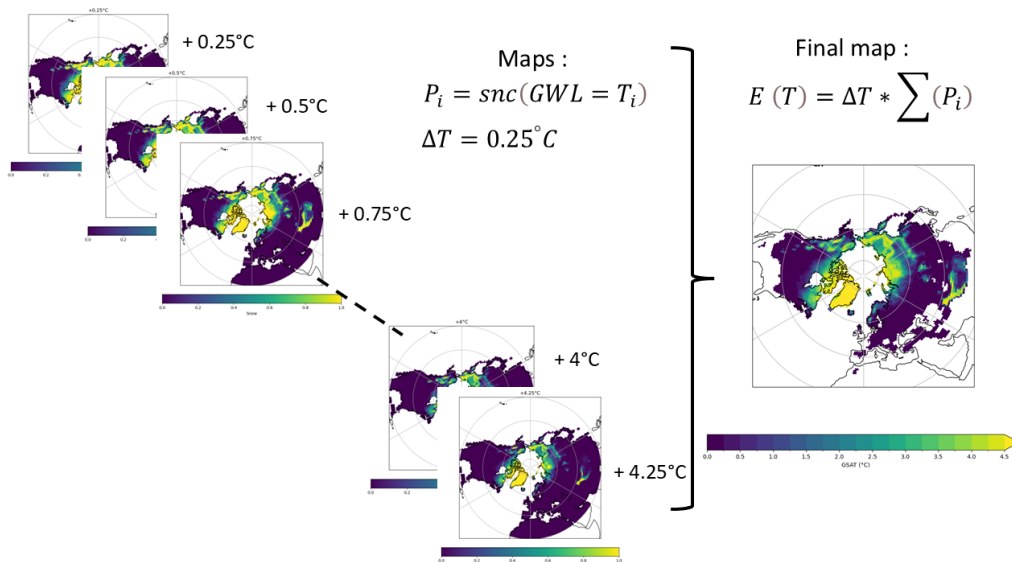


Figure 4: Schematic illustration of the binning procedure used to generate snow cover maps for each GWL. The example shown here was produced using the MRI-ESM2-0 model.

2.2.3 OpenReproLab

As part of the internship, a working group was formed with nine other interns and a high number of speakers to support us in making our work reproducible and to deepen our understanding of open science principles. This group called “OpenReproLab”, was specifically designed to promote open and reproducible scientific practices. Weekly meetings were organized, each focusing on a specific theme related to reproducibility.

This initiative provided us with access to a JupyterLab server with significant storage capacity, enabling collaborative and remote work. Throughout these sessions, we were trained in best practices such as modular programming, function creation, proper documentation, and sharing code and data. The aim was not only to apply these principles during the internship, but also to integrate them into our future professional practices. In this context, all of my scripts have been developed in accordance with these principles.

The code and analysis scripts developed during this internship will be made available at this link : https://github.com/vaysset1/M2_internship.

3 Results

3.1 Model selection

3.1.1 Snow cover agreement

As explained in the methods section, snow cover extent can either be obtained directly from the snow cover fraction (snc) variable or recalculated from the snow mass (snw) variable. Here, we present a comparison between the two approaches in terms of their agreement on snow cover representation.

To allow a fair comparison with the figure based on snow mass, this map includes only the models that provide the snw variable in their outputs. This ensures that both maps are based on the same subset of models, with an identical maximum number.

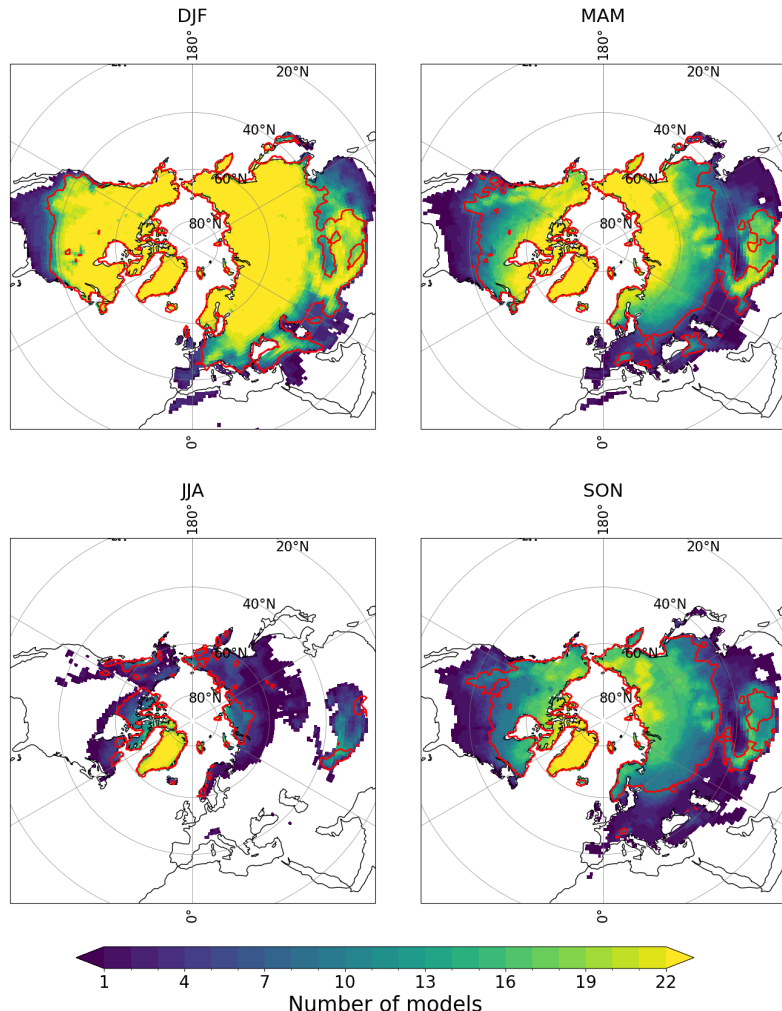


Figure 5: Seasonal snow cover agreement among CMIP6 models based on the snc variable. The color bar indicates the number of models simulating snow cover at each grid point. The red contour shows observational snow extent. (Inspired by IPCC (2007))

First, we can observe that the spatial distribution of snow varies depending on the model used

(fig. 5). Regions where all models agree in simulating snow are clearly identifiable as yellow areas on the maps. This suggests a good representation of snow cover by the models in these zones. Conversely, some regions show low model agreement, for example, in parts of Spain during winter and spring (fig. 5), where only a few models simulate snow cover.

Overall, the more the colors shift toward blue, the fewer models detect snow in that area.

Finally, the observed snow extent (represented by the red contours) generally follows the green to yellow zones of model simulations, indicating a coherent match between the models and the reference dataset.

The same set of maps was then generated using the recalculated snow cover based on snow mass data, identifying grid cells as snow-covered when the snow mass exceeds 5 kg/m^2 . These new maps (fig. 6) display fewer blue areas compared to those based on the original snc variable, indicating that models simulate snow cover more accurately when it is derived in a very simple manner from snow mass.

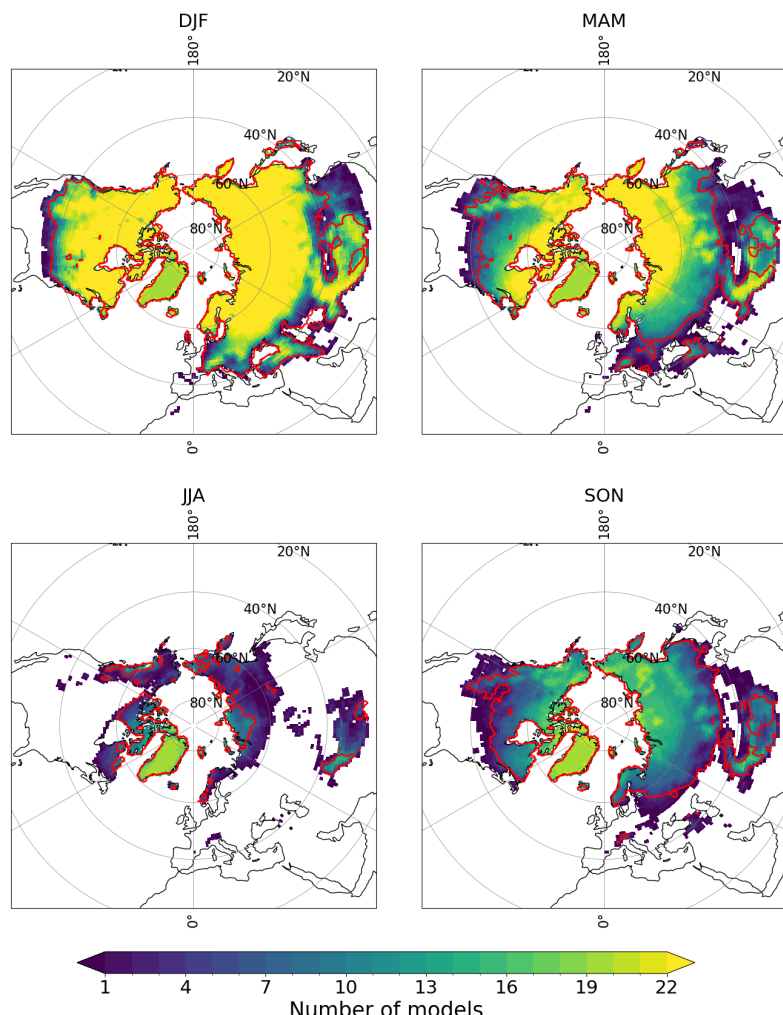


Figure 6: Seasonal snow cover agreement among CMIP6 models based on the snw variable. The color bar indicates the number of models simulating snow cover at each grid point. The red contour shows observational snow extent. (Inspired by IPCC (2007))

Improved results are particularly noticeable during winter and spring. The extent of simulated snow cover appears more realistic, with boundaries that are less exaggerated than in the previous method. Notably, unlike the earlier maps, these do not show extensive snow cover over Spain during winter and spring, a result that aligns more closely with observational data and expectations.

Despite these observations, the subsequent analyses will focus on the snc variable.

A more detailed comparison between the use of the snc variable and the snow mass-based approach will be provided in the Discussion section, with reference to previous studies.

3.1.2 Outlier detection

After a visual inspection, it is important to know exactly for which models the simulations are not good. In this sense, the boxplots representing the average monthly snow extent show consistent results. Here, these results were calculated using the two described methods : analyzing the historical simulations and examining the data according to GWL relative to 1995–2014. The two methods produced similar results in terms of average monthly snow extent (fig. 7).

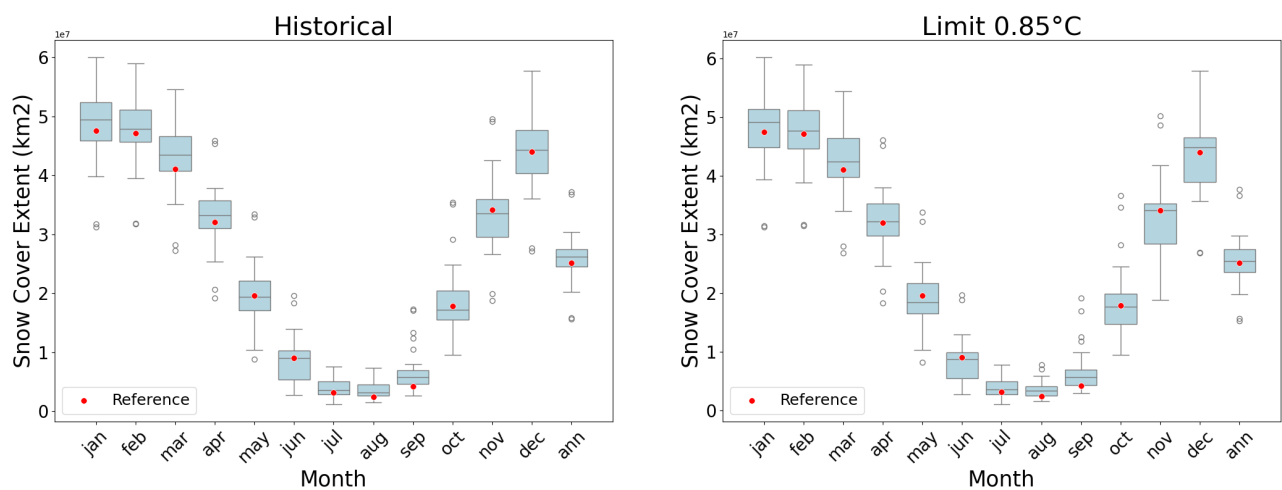


Figure 7: Boxplots representing the average monthly snow extent for two methods. Red points show observations.

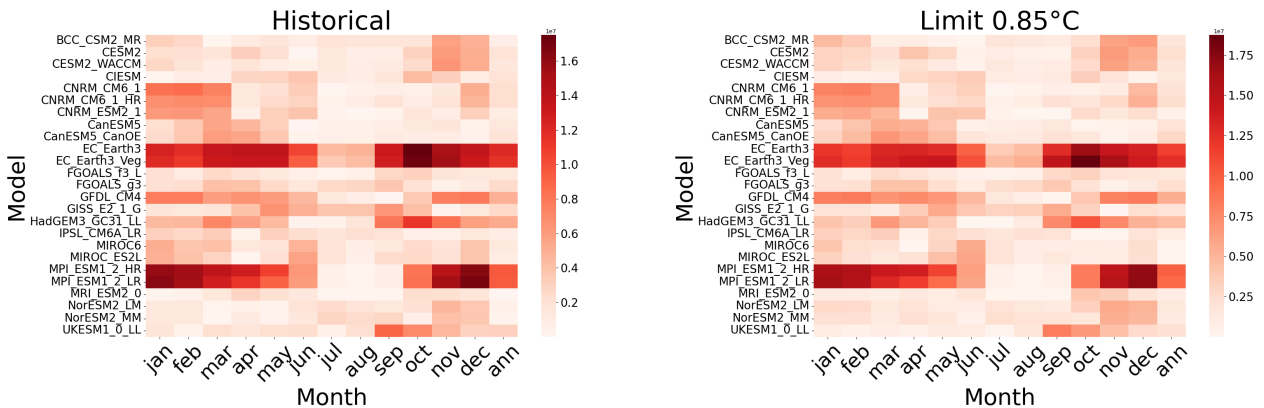
The values generally range between approximately 10 and $60 \times 10^6 \text{ km}^2$, depending on the month considered. While the distributions vary slightly from one month to another, the reference values consistently fall within the range of model outputs. This indicates a good overall agreement between the models and the observations.

In addition, a few outliers are present for each month. The models identified as outliers by both methods are listed in table 2.

Model	Month (Historical)	Month (Limit - 0.85 °C)
MPI-ESM1-2-HR	01, 02, 03, 04, 05, 11, 12, annual	01, 02, 03, 04, 05, 12, annual
MPI-ESM1-2-LR	01, 02, 03, 04, 11, 12, annual	01, 02, 03, 04, 12, annual
EC-Earth3	04, 05, 06, 09, 10, 11, annual	04, 05, 06, 08, 09, 10, 11, annual
EC-Earth3-Veg	04, 05, 06, 09, 10, 11, annual	04, 05, 06, 08, 09, 10, 11, annual
GISS-E2-1-G	09	
HadGEM3-GC31-LL	09, 10	09, 10
UKESM1-0-LL	09	09

Table 2: Outliers models for each method and month

Based on these results, absolute errors were calculated for each method. While the differences between the methods are sometimes small, they are not negligible. In both cases, the models with the highest errors include EC-Earth and MPI-ESM, as well as GFDL and, to a lesser extent, HadGEM3 (see fig. 8). These findings are consistent with the visual patterns previously observed in the boxplots.

**Figure 8:** Heatmaps showing absolute errors of both methods by month and model

These numerical visualizations have the advantage of clearly identifying models with poor performance, as highlighted by the evaluation maps. This facilitates an informed and transparent model selection process, ensuring that only the most reliable models are included in subsequent analyses.

3.1.3 Scoring results

Model	Average error (10^6 km 2)	Exponential scoring	Gaussian scoring
MRI-ESM2-0	1.27	1.000000	1.000000
FGOALS-f3-L	1.61	0.968784	0.991986
NorESM2-LM	1.85	0.947293	0.976818
NorESM2-MM	1.87	0.945724	0.975395
IPSL-CM6A-LR	1.93	0.940619	0.970464
CIESM	1.96	0.937564	0.967296
CanESM5	2.06	0.929402	0.958024
CanESM5-CanOE	2.18	0.918590	0.943948
CESM2-WACCM	2.20	0.917041	0.941764
BCC-CSM2-MR	2.29	0.909790	0.930991
CESM2	2.40	0.900656	0.916144
FGOALS-g3	2.43	0.897737	0.911101
CNRM-ESM2-1	2.65	0.879724	0.876889
MIROC6	2.78	0.868940	0.853953
MIROC-ES2L	2.79	0.868178	0.852264
UKESM1-0-LL	3.10	0.843928	0.794253
CNRM-CM6-1-HR	3.18	0.837750	0.778231
CNRM-CM6-1	3.30	0.828307	0.752864
GISS-E2-1-G	3.37	0.823082	0.738404
GFDL-CM4	4.96	0.709852	0.390808
HadGEM3-GC31-LL	5.21	0.694085	0.344129
MPI-ESM1-2-LR	9.42	0.469709	0.010379
MPI-ESM1-2-HR	9.60	0.461875	0.008450
EC-Earth3-Veg	1.15	0.385663	0.000701
EC-Earth3	1.21	0.367879	0.000335

Table 3: Scoring results for each model

The scores obtained from the exponential and Gaussian scoring are presented in table 3. While both methods yield similar scores for models that accurately simulate observed conditions, larger discrepancies appear for models with poor performance.

For example, with exponential scoring, even poorly performing models retain relatively high scores (a minimum of 0.37). In contrast, Gaussian scoring strongly penalizes these models, with scores dropping as low as 0.00033 for the same case (table 3).

This raises an important question: which scoring function is better suited to produce the most reliable weighted multi-model mean?

Visually (see fig. 16 in annex section), we observe that models with good performance tend to produce similar results and thus receive relatively close scores. In contrast, poorly performing models often overestimate or underestimate snow extent, which can distort the multi-model mean if they are assigned a high weight.

While some degree of compensation might occur between over- and underestimating models, relying on this effect introduces unnecessary uncertainty, it is therefore preferable to minimize the influence of unreliable models.

Additionally, models such as GFDL and HadGEM3, which show significant errors for specific months, still receive scores comparable to better-performing models when using exponential scoring. However, Gaussian scoring assigns them much lower weights, reflecting their reduced reliability.

3.2 Multi-model mean

3.2.1 Multi-model methods comparison

To assess which method provides the most accurate simulation of future snow extent, it is essential to evaluate how well each method reproduces historical values. As an example, we focused on the winter season and computed the average snow cover extent using four different methods (fig. 9). In all cases, snow is considered to be present at a given location and time when it covers at least 15% of the area.

Using a simple multi-model mean, we observe an overestimation of snow cover, particularly along the southern boundary of North America and in China (fig. 9). This overestimation is less pronounced in the other methods, where snow cover is better simulated in southern North America. However, the overestimation over China appears in all methods, although it is reduced in the exclusion and Gaussian-weighted approaches. The most accurate estimate appears to be produced by the weighted mean using Gaussian scoring, which closely follows the reference snow line, especially in North America and Europe (fig. 9).

However, the method based on excluding poorly performing models (those for which the relative error is superior to 20%) (fig. 9) also provides a realistic estimate of snow cover, offering a robust alternative. This suggests that a targeted model selection strategy can yield reliable results.

When examining the numerical values (table 4), the simple mean using all models yields the greatest deviation from the reference dataset. In contrast, the best-performing methods are the exclusion-based approach and the weighted mean with Gaussian scoring. These results indicate that removing underperforming models may serve as a solid first approximation for improving snow

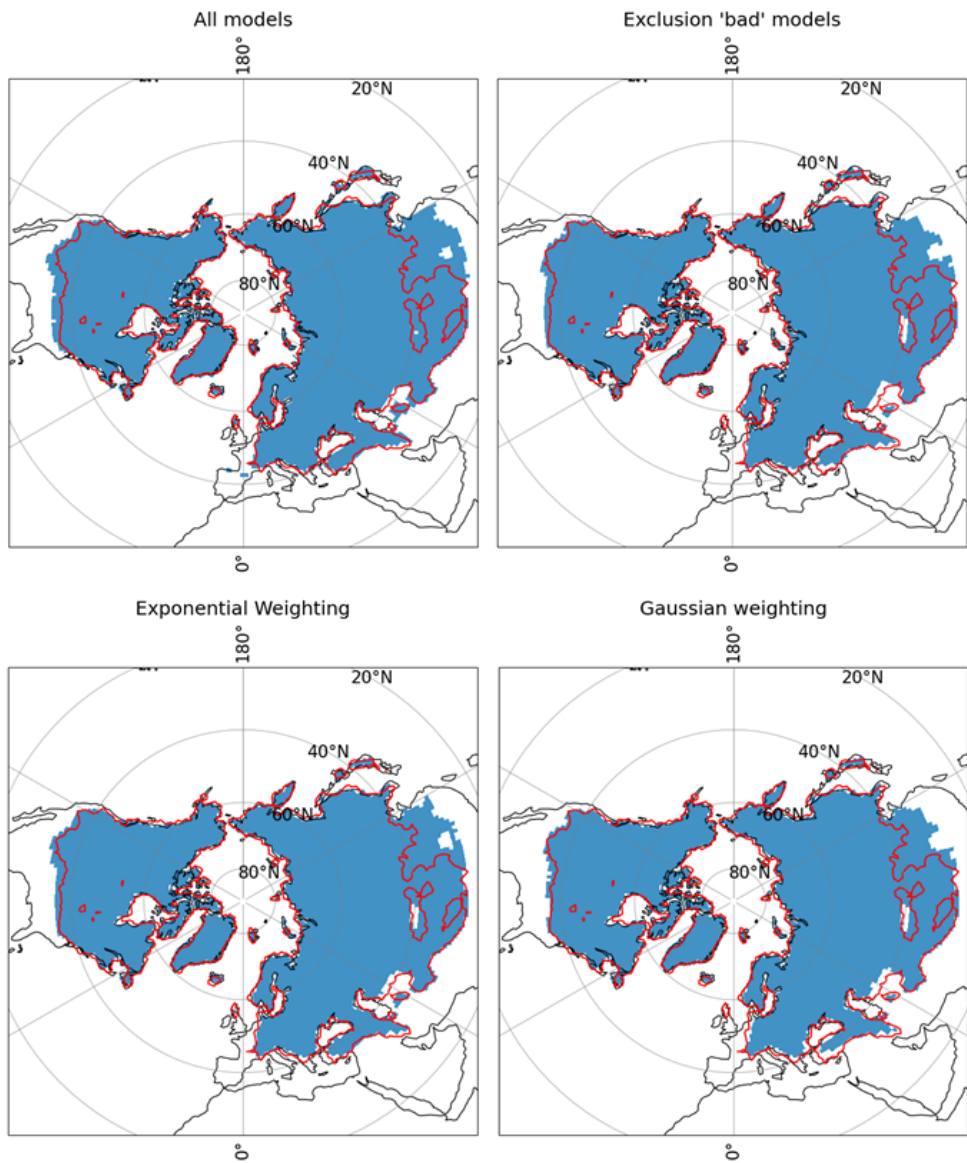


Figure 9: Average winter snow cover during the reference period (1995-2014) based on the CMIP6 multi-model ensemble using four different methods. (A) Simple mean of all models, (B) Simple mean excluding poorly performing models, (C) Weighted mean with exponential scoring, and (D) Weighted mean with Gaussian scoring. The red contour represents the reference snow extent for the same period.

cover simulations.

Method	Snow cover extent (10^6 km 2)
All models	56.4
Exclusion of poor models	54.0
Weighted mean with exponential scoring	54.3
Weighted mean with Gaussian scoring	53.1
Reference	52.5

Table 4: Average winter snow cover extent during the reference period (1995-2014) for the four different multi-model mean methods and the reference.

Despite these differences, the results remain relatively close across the different methods, as only a few models significantly very substantially misrepresent the present-day snow cover.

Among the available approaches, the Gaussian scoring appears more selective and effectively limits the contribution of poorly performing models without excluding them entirely. For this reason, it will be used in the following analyses.

3.2.2 Seasonal snow extension

Based on the Gaussian scoring function, the multi-model mean has been applied on snow cover values. fig. 10 shows the seasonal evolution of the snow cover depending on the GWL relative to the 1995-2014 period.

Globally, for each season (except in some parts of China), observations indicate greater snow cover than all model simulations.

During the winter, model simulations at -0.5°C GWL closely follow observations over the North American and European continents, but less so in Asia. In spring, the opposite pattern is observed: at -0.5°C GWL, model simulations align better with observations in Europe and Asia than in North America, a pattern that also holds for autumn. In summer, snow persists only in Greenland, on the borders of the American and European continent and in Nepal.

The other key observation is that snow loss with warming is approximately linear only up to +3°C. At +4°C, the snow boundary shifts much more compared to the changes observed between lower warming levels. This non linear response is especially pronounced in spring and autumn, but also notable in winter. During summer, snow remains present only in Greenland, compared to lower GWLs.

After visual observations, numerical values have been calculated for each season and GWL. All the exact values are reported in table 5 in annex. Numerical values confirm what it was observed in maps (fig. 11).

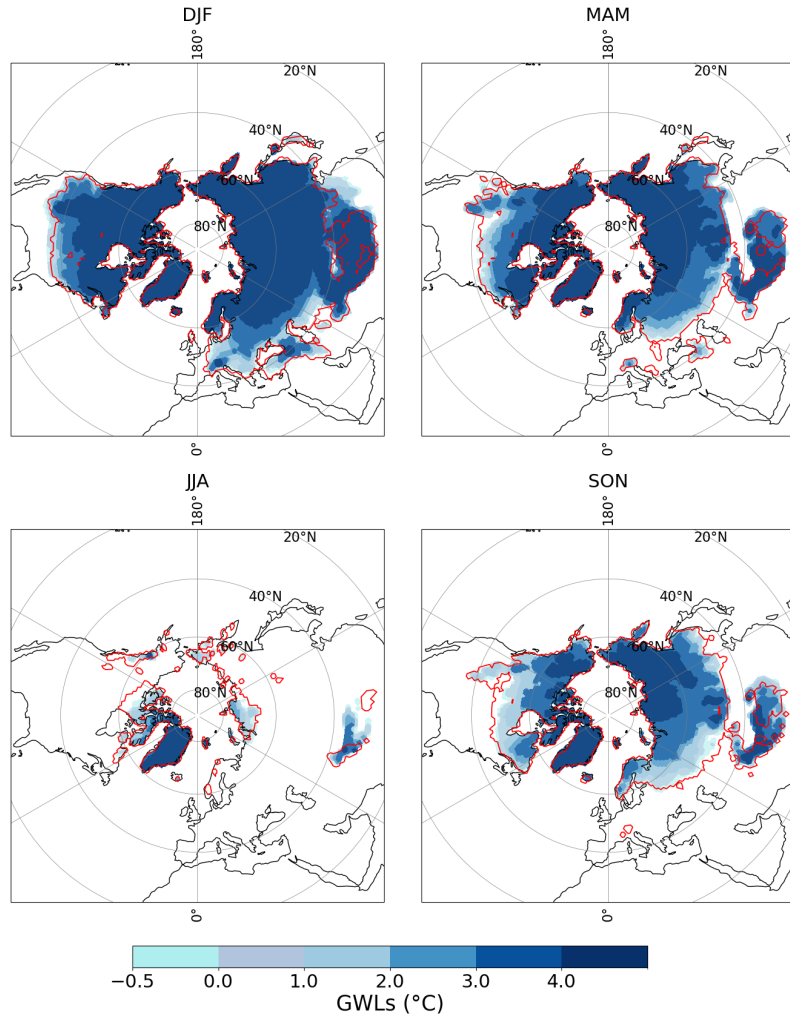


Figure 10: Seasonal projected snow cover in function of the global warming level from a multi-model mean of CMIP6 models. Each color corresponds to a different warming. The red contour shows observations (1995-2014). DJF : Winter, MAM : Spring, JJA : Summer, SON : Autumn.

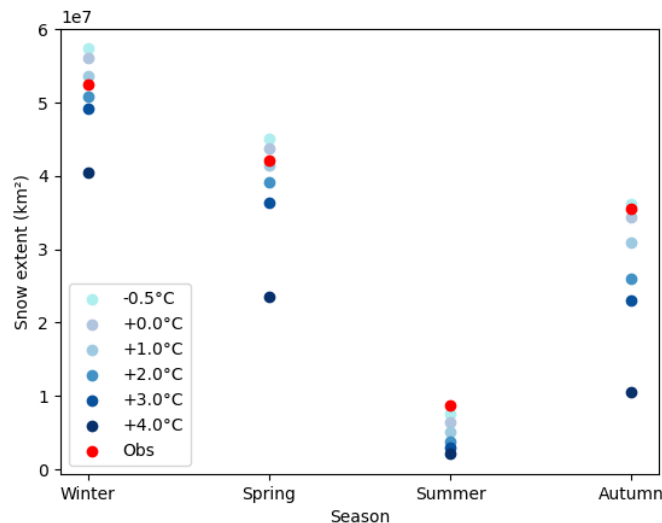


Figure 11: Seasonal values of the snow cover extent (km^2) for each GWL. Each blue color represents a different warming and the red corresponds to the observations.

In winter and spring, we observe that snow cover extent decreases gradually between -0.5 and +3°C of global warming, varying between 57 and 49.10^6 km^2 in winter and from approximately 45 and 36.10^6 km^2 in spring. Once the GWL reaches +4°C, a sharp decline is observed. In spring, snow cover drops from 36 to 23.10^6 km^2 (-36%) and in winter from 49 to 41.10^6 km^2 (-16%), despite only one additional degree of warming. It is also the case in autumn, where snow cover decreases from 23 to 11.10^6 km (-52%) between +3 and +4°C. These results suggest the existence of a threshold around +3°C, beyond which snow extent decreases more rapidly.

In summer, values are very low, between 2 and 7.10^6 km^2 , limiting the relevance of observations for this season.

To talk in terms of snow cover extent change relative to the 1995-2014 reference period, in function of GWLs, a similar figure to the first one (fig. 1) was produced for each season (fig. 12).

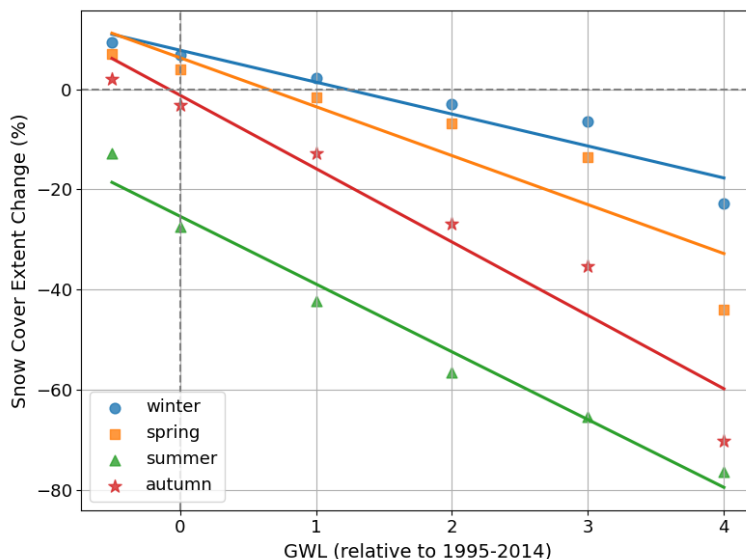


Figure 12: Seasonal snow cover extent change in function of GWLs, relative to 1995-2014 period.
Blue : Winter, Orange : Spring, Green : Summer, Red : Autumn.

This figure reveals consistent values for winter, spring and autumn, with near-zero changes at 0°C and even an increase in snow extent during slight cooling.

In contrast, for summer, values are already negative at 0°C, indicating possible misrepresentation of snow cover for this season.

A key observation for winter, spring and autumn is the relatively linear decline in snow cover from -0.5 to +3°C of warming, as also illustrated in fig. 1. The decline becomes much steeper at +4°C, in line with the patterns observed in the spatial distribution maps.

In spring, snow cover decreases by approximately 14% between 0 and +3°C (relative to 1995-2014), and by more than 40% at +4°C. In winter, the decrease is less than 6% between 0 and +3°C , but exceeds 20% at +4°C. In autumn, snow cover declines by over 35% between 0 and +3°C and by more than 70% at +4°C.

This sharp contrast is less pronounced in summer, where the decline appears more linear across warming levels, although total snow loss remains very high at +4°C.

3.2.3 Seasonal snow cover with a selection of models

As we observed a sharp snow cover decline between +3 and +4 °C (relative to 1995-2014), we reproduced the same maps using only the subset of models that simulate snow cover up to at least +3.5 °C of global warming relative to the same baseline (16 models). The goal is to assess whether the number of models contributing at each GWL affects the multi-model mean. The excluded models are the following : BCC-CSM2-MR, FGOALS-g3, GISS-E2-1-G, MIROC6, MIROC-ES2L, MPI-ESM1-2-HR/LR and NorESM2-LM/MM.

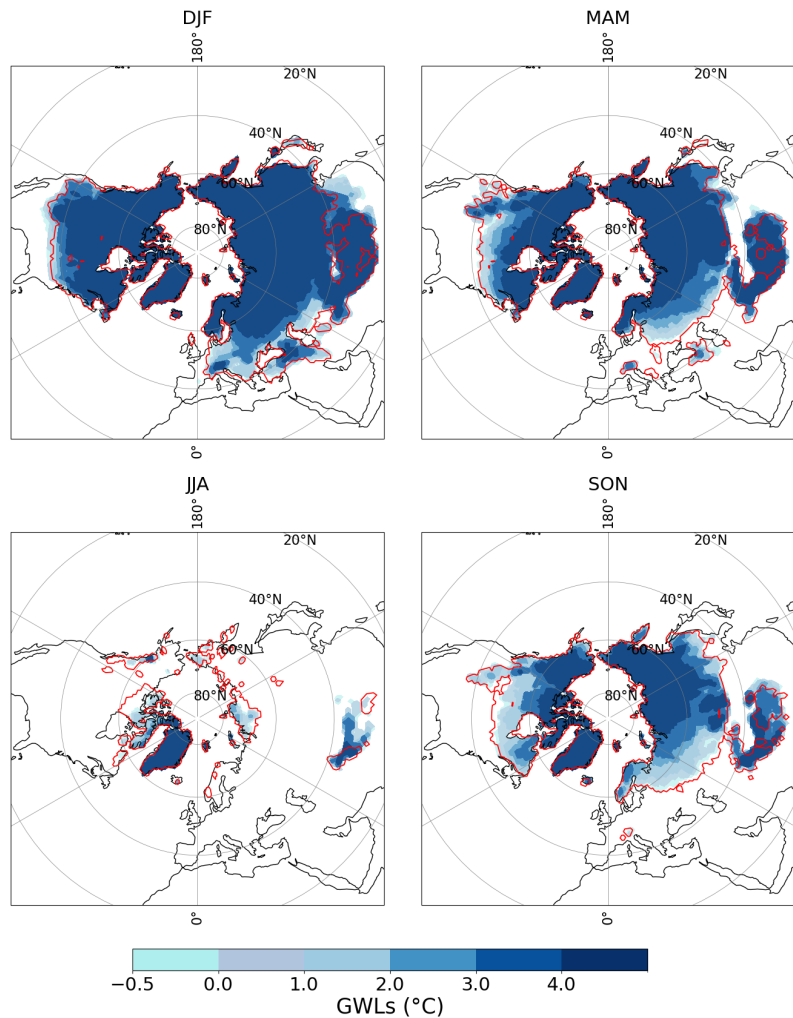


Figure 13: Seasonal projected snow cover in function of the global warming level from a multi-model mean of 16 CMIP6 models simulating snow up to +3.5 °C. Each color corresponds to a different warming. The red contour shows observations (1995-2014). DJF : Winter, MAM : Spring, JJA : Summer, SON : Autumn.

On this new map, we observe main differences. The decline is less sharp between +3 and +4 °C during winter (fig. 13), and snow cover persists over large parts of Eurasia and North America at +4 °C during spring (fig. 13) compared to the map with all models during this season (fig. 10). No big differences are noticeable during summer and autumn.

These differences are confirmed by numerical values (fig. 14).

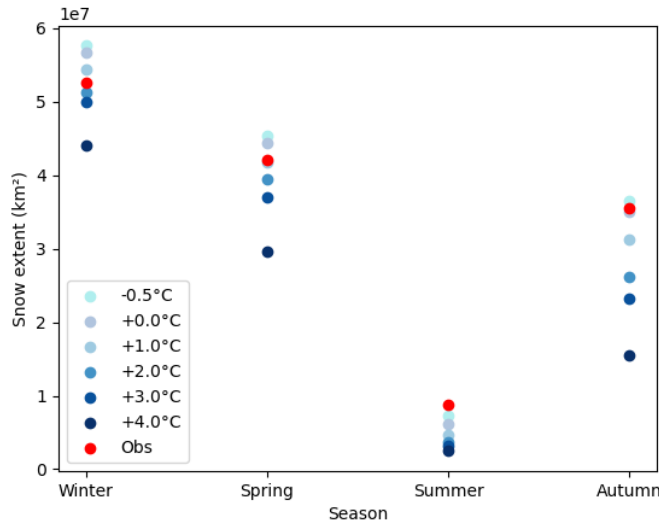


Figure 14: Seasonal values of the snow cover extent (km^2) for each GWL. Each blue color represents a different warming and the red corresponds to the observations.

When the GWL reaches $+4^\circ\text{C}$, the winter snow cover drops from 50 to 44.10^6 km^2 and during spring from 37 to 30.10^6 km^2 , a decline smaller than when all models are taken into account. Similarly, in autumn, the drop between $+3^\circ\text{C}$ and $+4^\circ\text{C}$ is also less pronounced in this subset.

This reduced contrast across warming levels suggests that the sharp decline observed previously may be partly influenced by the changing composition of the model ensemble at higher GWLs ($+3^\circ\text{C}$ and $+4^\circ\text{C}$, relative to the present period 1995-2014). While some variation is expected due to the number of models available at each warming level, such a strong effect raises questions about the robustness of the multi-model mean at $+4^\circ\text{C}$. This issue is likely methodological and will be further discussed in the following sections.

3.2.4 Evolution of the snow extent compared to 1850-1900 period

Up to this point, all the results presented have shown the evolution of snow cover extent as a function of GWL relative to the 1995-2014 reference period. In this case, the map displays similar results, but using 1850-1900 as the reference period instead.

This final map (fig. 15) closely resembles the previous one, with a noticeable shift in isotherms of approximately 1°C . This shift corresponds to the global warming difference between the two reference periods, estimated at $+0.85^\circ\text{C}$ (IPCC (2021)).

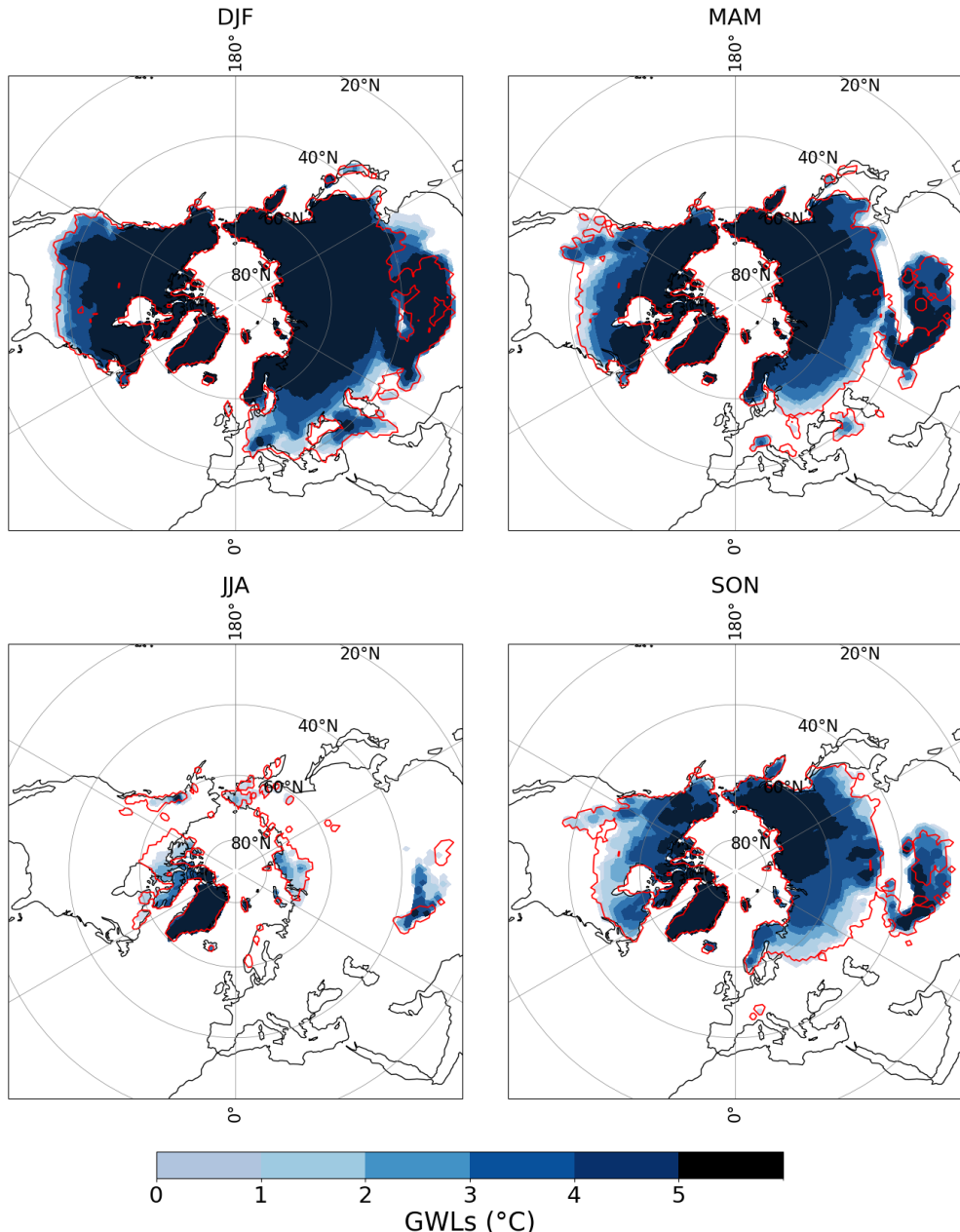


Figure 15: Seasonal projections of snow cover extent as a function of the global warming levels (relative to 1850-1900) from a multi-model mean of CMIP6 models. Each color corresponds to a different warming. The red contour indicates observations (1995-2014). DJF : Winter, MAM : Spring, JJA : Summer, SON : Autumn.

4 Discussion

4.1 Snow variables and representation issues in climate models

As introduced at the beginning of this report, snow plays a key role in the climate system through two main mechanisms. First, snow acts as an insulator for the soil (Gouttevin et al. (2012)). This insulating property depends essentially on snow height and density, and is thus parameterized as a function of snow mass (snw) in many climate models. The second mechanism is the effect of snow cover on surface albedo. Snow reflects a significant portion of incoming solar radiation. The total reflected incoming solar radiation is therefore largely determined by the snow cover fraction (variable snc) in models (Flanner et al. (2011)). Although both effects are important, one may question which is more relevant for assessing snow distribution in climate models. Some studies have proposed using snw to recalculate the snow cover fraction, considering snow to be present when the snow mass exceeds 5 kg/m² (Brutel-Vuilmet et al. (2013)), compensating for errors in the parameterization of the snow cover fraction as a function of the snow mass (e.g., Lalande et al. (2023)). Comparisons between snc-based and snw-based snow cover estimates show that the snow mass approach tends to provide more consistent results across models, with greater agreement on the spatial extent of simulated snow. However, since snc is the variable directly involved in the surface energy budget, it should, in principle, be well-represented. Yet, model outputs reveal that this is not the case for all models ; for example, EC-Earth3 exhibits a particularly poor snow cover extent representation. These discrepancies may arise from model formulation or from issues in post-processing or output writing. Since such biases are also reflected in comparisons with observations and quite possibly degrade the simulated local and global energy balance in the model itself, they justify the exclusion of certain models from further analysis.

4.2 Final model selection and weighting strategy

Given the presence of poorly performing models, careful model selection is essential. Three selection methods were tested: (1) excluding models with the worst performance relative to observations (four models in this case), and two more gradual scoring approaches (exponential and Gaussian). As discussed in the methods section, an effective scoring function should reward high-performing models while clearly penalizing poor ones.

As presented in the results, the different multi-model methods seem to give near results (see section 3.2.1). Especially, when we select some models by excluding the poor ones, the results are quite similar to those obtained by the Gaussian weighting method. Despite these observations, we chose the Gaussian scoring because it is the only method which takes all models into account, but strongly penalizes the ones that are less good in simulating observed snow. This choice is also less arbitrary, as the Gaussian function (despite having a single parameter), remains relatively simple and interpretable.

This method has both advantages and drawbacks. A major advantage is that low-performing models have minimal influence on the final multi-model mean. The main drawback lies in the uncertainty of the scoring method itself; there is no absolute guarantee that it captures model realism perfectly. The choice, while partly subjective, is nonetheless grounded in sound scientific reasoning and transparent

criteria. The effect is not strong, but it confirms the robustness of the analysis.

4.3 Impact of snow threshold and model sampling on results

It is important to discuss another methodological choice. A threshold of 15% was used to consider snow as present at a given time and location. This decision followed a reflection, and an alternative test was performed using a 50% threshold (fig. 17 in annex). The main observation is that snow cover extent is highly sensitive to this choice, values differ significantly between the two approaches. The final choice of the 15% threshold was supported by several studies. It is used in remote sensing to distinguish areas with light snow cover from signal noise (Riggs et al. (2022)). An analogy can also be drawn with sea ice. As mentioned in the introduction, snow and sea ice exhibit similar responses to temperature. Consequently, the threshold commonly used for sea ice detection (15%) (Matthews et al. (2020)) is assumed to be valid for snow. That said, using a 50% threshold can also be justified if one considers snow to be present only when it occurs in at least half of the time steps, but this definition remains quite relative.

When examining the final maps of future snow cover projections, a key observation emerges: a threshold appears around +3 °C, beyond which snow declines more rapidly. This is surprising, as studies like the IPCC (fig. 1) generally suggest a linear decrease. This sharp drop between +3 and +4 °C is less intense when the number of models is reduced, because not all models simulate snow at every GWL. However, this change in model availability should not significantly affect the final representation, which may point to a methodological issue in the calculations.

4.4 Scenario dependence and robustness of results

All analyses in this study were conducted using simulations from the SSP5-8.5 scenario. One may question whether changing the scenario would alter the results. However, as shown in fig. 1, linear trends in snow cover extent appear similar across different SSPs, indicating that results would be largely consistent regardless of the specific pathway. SSP5-8.5 was chosen because it reaches the highest level of warming (+5 °C GWL), allowing the exploration of the full range of possible changes. Despite recent criticisms of this scenario, particularly as assessments suggest it is increasingly unlikely given current and projected global emissions trends (Hausfather and Peters (2020)), these concerns do not affect the robustness of our findings, since similar behaviors are observed across different pathways.

This debate around high-emissions scenarios has also received attention in policy circles, particularly in the United States (White House (2025)). For example, recent official documents have raised concerns about scenarios such as RCP8.5, highlighting that some of their assumptions may no longer align with present-day energy and emissions trajectories. This has led to broader discussions on the appropriate role of climate scenarios in decision-making.

Nevertheless, such debates primarily concern long-term projections for mitigation policy, and do not undermine the validity of our approach. Since our study focuses on the sensitivity of snow cover to global warming levels, the choice of scenario does not compromise the robustness of the results.

5 Conclusion and Outlooks

This study has produced future snow cover extent projections based on global warming levels (GWLs), using different multi-model mean methods. The final method selected was the Gaussian-weighted multi-model mean, which offers the advantage of incorporating all available models while reducing the influence of those that perform poorly against observations. One of the objectives was to assess whether this approach is scientifically sound. The final results suggest that it provides coherent and consistent outcomes.

However, the analysis also highlights that several factors can significantly influence the results, including the choice of method, the variable used (snc or snw), the threshold applied to define snow presence (e.g., 15 or 50%), and the number of models able to simulate snow cover at different GWLs. Each of these aspects introduces a degree of sensitivity that needs to be considered in the interpretation of the results.

To further improve the robustness of the findings, future research could explore in more depth the role of the number of models contributing at each GWL. In theory, this should not strongly impact the results, but as observed, it may partly explain the nonlinear behavior between +3 and +4 °C. A deeper investigation of this threshold could provide insights into nonlinear responses of snow cover to warming.

Finally, the approach developed in this study could be extended to other components of the cryosphere, such as sea ice or permafrost, in order to provide a more comprehensive understanding of climate change impacts on the Northern Hemisphere cryosphere.

References

- Brutel-Vuilmet, C., Ménégoz, M., and Krinner, G. (2013). An analysis of present and future seasonal Northern Hemisphere land snow cover simulated by CMIP5 coupled climate models. *The Cryosphere*, 7(1):67–80.
- Estilow, T. W., Young, A. H., and Robinson, D. A. (2015). A long-term Northern Hemisphere snow cover extent data record for climate studies and monitoring. *Earth System Science Data*, 7(1):137–142.
- Eyring, V., Bony, S., Meehl, G. A., Senior, C. A., Stevens, B., Stouffer, R. J., and Taylor, K. E. (2016). Overview of the Coupled Model Intercomparison Project Phase 6 (CMIP6) experimental design and organization. *Geoscientific Model Development*, 9(5):1937–1958.
- Flanner, M. G., Shell, K. M., Barlage, M., Perovich, D. K., and Tschudi, M. A. (2011). Radiative forcing and albedo feedback from the Northern Hemisphere cryosphere between 1979 and 2008. *Nature Geoscience*, 4(3):151–155.
- Gouttevin, I., Menegoz, M., Dominé, F., Krinner, G., Koven, C., Ciais, P., Tarnocai, C., and Boike, J. (2012). How the insulating properties of snow affect soil carbon distribution in the continental pan-Arctic area. *Journal of Geophysical Research: Biogeosciences*, 117(G2):2011JG001916.
- Hausfather, Z. and Peters, G. P. (2020). Emissions – the ‘business as usual’ story is misleading. *Nature*, 577(7792):618–620.
- IPCC (2007). *Climate Change 2007 – The Physical Science Basis: Contribution of Working Group I to the Fourth Assessment Report of the Intergovernmental Panel on Climate Change*. Cambridge University Press, Cambridge, United Kingdom and New York, NY, USA, 1 edition.
- IPCC (2013). *Climate Change 2013 – The Physical Science Basis: Working Group I Contribution to the Fifth Assessment Report of the Intergovernmental Panel on Climate Change*. Cambridge University Press, 1 edition.
- IPCC (2021). *Climate Change 2021 – The Physical Science Basis: Working Group I Contribution to the Sixth Assessment Report of the Intergovernmental Panel on Climate Change*. Cambridge University Press, 1 edition.
- Lalande, M., Ménégoz, M., Krinner, G., Ottlé, C., and Cheruy, F. (2023). Improving climate model skill over High Mountain Asia by adapting snow cover parameterization to complex-topography areas. *The Cryosphere*, 17(12):5095–5130.
- Matthews, J. L., Peng, G., Meier, W. N., and Brown, O. (2020). Sensitivity of Arctic Sea Ice Extent to Sea Ice Concentration Threshold Choice and Its Implication to Ice Coverage Decadal Trends and Statistical Projections. *Remote Sensing*, 12(5):807.
- Mudryk, L., Santolaria-Otín, M., Krinner, G., Ménégoz, M., Derksen, C., Brutel-Vuilmet, C., Brady, M., and Essery, R. (2020). Historical Northern Hemisphere snow cover trends and projected changes in the CMIP6 multi-model ensemble. *The Cryosphere*, 14(7):2495–2514.
- Riggs, G., Hall, D., Vuyovich, C., and DiGirolamo, N. (2022). Development of Snow Cover Frequency Maps from MODIS Snow Cover Products. *Remote Sensing*, 14(22):5661.

Annex

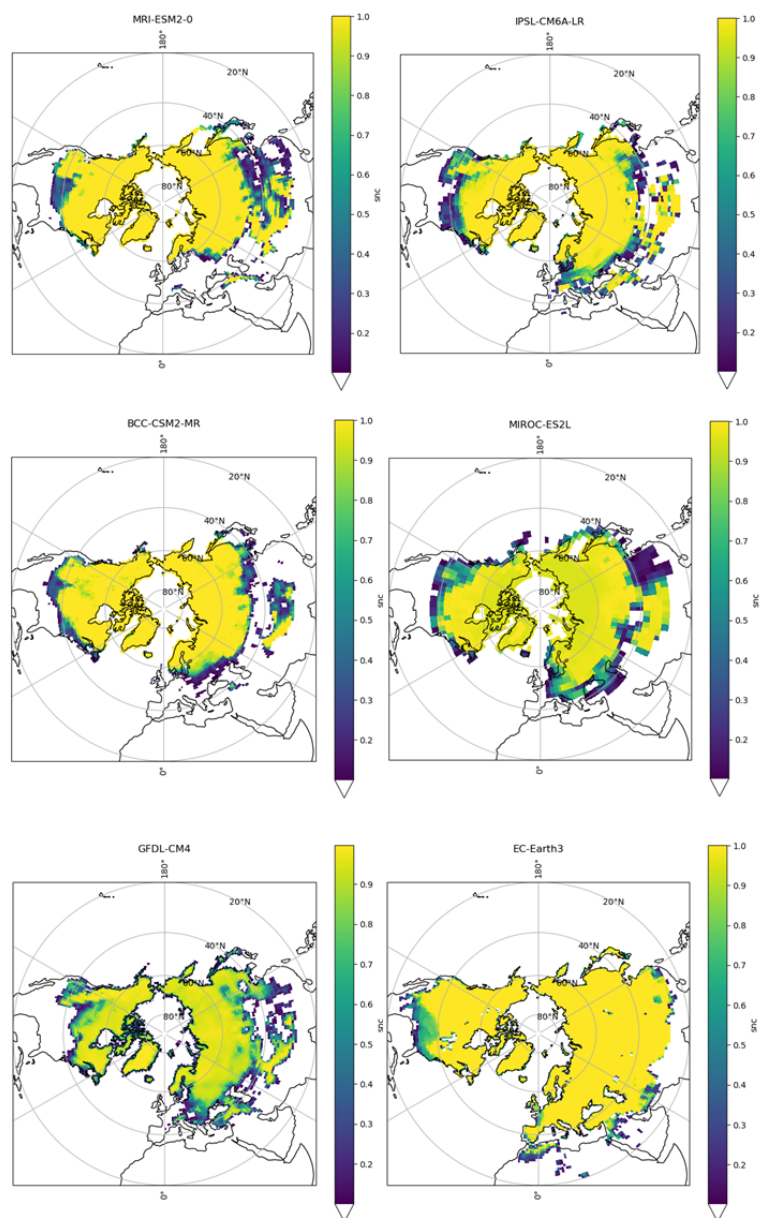


Figure 16: Snow cover extent simulations from 6 different models of CMIP6 ensemble : MRI-ESM2-0, IPSL-CM6A-LR, BCC-CSM2-MR, MIROC-ES2L, GFDL-CM4, EC-Earth3

GWLS (°C)	Snow Cover Extent (km²)
-0.5	57.4×10^6
0	56.1×10^6
1	53.7×10^6
2	50.9×10^6
3	49.1×10^6
4	40.5×10^6

Table 5: Winter snow cover extent (km²) as a function of Global Warming Levels (GWLS)

GWLS (°C)	Snow Cover Extent (km²)
-0.5	45.1×10^6
0	43.8×10^6
1	41.5×10^6
2	39.3×10^6
3	36.4×10^6
4	23.6×10^6

Table 6: Spring snow cover extent (km²) as a function of Global Warming Levels (GWLS)

GWLS (°C)	Snow Cover Extent (km²)
-0.5	7.6×10^6
0	6.4×10^6
1	5.1×10^6
2	3.8×10^6
3	3.0×10^6
4	2.1×10^6

Table 7: Summer snow cover extent (km²) as a function of Global Warming Levels (GWLS)

GWLS ($^{\circ}\text{C}$)	Snow Cover Extent (km^2)
-0.5	36.2×10^6
0	34.4×10^6
1	30.9×10^6
2	25.9×10^6
3	23.0×10^6
4	10.6×10^6

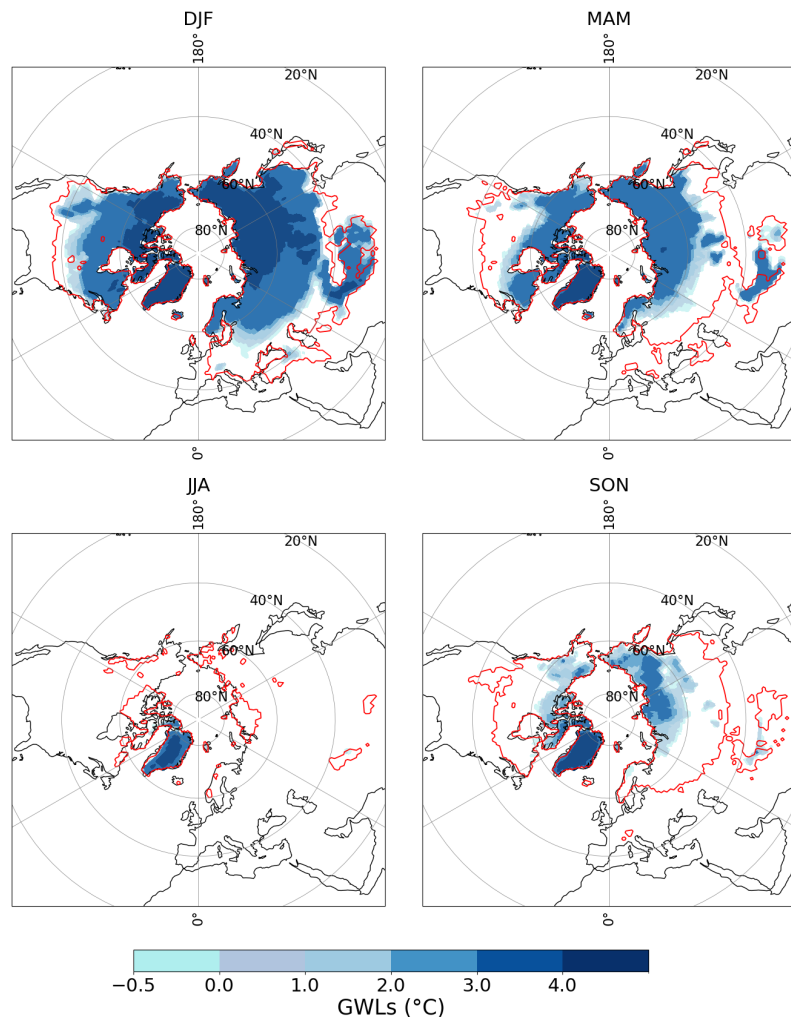
Table 8: Autumn snow cover extent (km^2) as a function of Global Warming Levels (GWLS)

Figure 17: Seasonal projections of snow cover extent as a function of the global warming levels (relative to 1850-1900) from a multi-model mean of CMIP6 models, with a 50% threshold. Each color corresponds to a different warming. The red contour indicates observations (1995-2014). JJA : Winter, MAM : Spring, JJA : Summer, SON : Autumn